

From antinode clusters to node clusters: The concentration dependent transition of floaters on a standing Faraday wave

Ceyda Sanli,^{*} Detlef Lohse,[†] and Devaraj van der Meer[‡]
*Physics of Fluids Group, MESA+ Institute for Nanotechnology,
 J. M. Burgers Centre for Fluid Dynamics, University of Twente,
 P.O. Box 217, 7500 AE Enschede, The Netherlands*

(Dated: March 11, 2019)

A hydrophilic floating sphere which is denser than water drifts to an amplitude maximum (antinode) of a surface standing wave. A few identical floaters therefore organize into antinode clusters. However, beyond a transitional value of the floater concentration ϕ , we observe that the same spheres spontaneously accumulate at the nodal lines, completely inverting the self-organized particle pattern on the wave. From a potential energy estimate we show (i) that at low ϕ antinode clusters are energetically favorable over nodal ones and (ii) how this situation reverses at high ϕ , in agreement with the experiment.

PACS numbers: 47.54.-r, 47.35.-i, 45.70.-n, 05.65.+b

Introduction – A small sphere floating at a water-air interface exhibits fascinating behavior when exposed to a periodic oscillation: On a standing surface wave, the floater moves either towards an amplitude maximum (antinode) or to an amplitude minimum (node). Whether a floater moves to the antinode or the node is determined by both the floater density relative to that of the carrier liquid and the floater hydrophobicity [1–3]: If the floater mass is larger than the displaced liquid mass the floater drifts towards the antinode, and in the reverse case it moves towards the node [4]. This drift continues throughout each wave period until the floater reaches a steady state position, either at an antinode or at a nodal line [1–3].

Thus, the dynamics of a single floater on a standing wave is quantitatively understood and node clusters of a few hydrophilic light floaters have been observed [1–3]. On the other hand, the behavior of densely packed monolayers of floaters –so-called floater (or particle) rafts [5] on a quiescent surface are shown to be dominated by the attractive capillary interaction among the floaters [6, 7]. These lead to heterogeneity of the floater packing [8], and both granular and elastic responses of the floater raft [5]. In addition, the response of such a floater raft to a traveling capillary wave has been studied, in order to determine its elastic properties [9].

In this Letter, we combine the above two independent research problems into a single experiment: We study the position of hydrophilic heavy floaters on a standing Faraday wave as a function of the floater concentration ϕ , by simply adding additional floaters to the surface. We experimentally show that the position of the floaters highly depends on ϕ . For low ϕ , our floaters accumulate at the antinodes as –for the particles used in this experiment– would be expected from theory [1, 3] and

previous experiments [1–3]. Increasing ϕ , we observe that the same hydrophilic heavy floaters cluster around the nodal lines. Importantly, we show that this inverted clustering is *not* due to an inverted drift of a single floater, but arises as a *collective effect* of many interacting floaters. Subsequently, we develop a potential energy estimate to explain why for high values of ϕ nodal clusters are energetically favored over the antinodal ones.

Experiment – The experimental setup is illustrated in Fig. 1. A container, made from transparent hydrophilic glass with 10 mm height and 81×45 mm² rectangular cross section is attached to a shaker. The container is completely filled with purified water (Millipore water with a resistivity > 18 M Ω -cm) such that the water level is perfectly matched with the container edge [Fig. 1(f)]. Using this so-called brim-full boundary condition [10], a static surface inclination induced by the boundary is avoided [1–3]. Spherical polystyrene floaters [11] (contact angle 74° [12] and density 1050 kg/m³) with average radius R around 0.31 mm and a polydispersity of approximately 14% are carefully distributed over the water surface to make a monolayer. To avoid surfactant effects, we clean both the container and the floaters by performing the cleaning protocol described in [13].

A standing Faraday wave is generated using a shaker providing a vertical sinusoidal oscillation with amplitude a_0 and frequency f_0 . We determine f_0 such that we produce a rectangular wave pattern with a wavelength in the range of 17 to 24 mm corresponding to frequencies ranging from 37 to 42 Hz (note that the standing Faraday wave frequency is equal to $f_0/2$). Adding floaters to the surface, we need to slightly adjust both a_0 and f_0 to obtain a well defined rectangular pattern [14]. A continuous white fiber-light source (Schott) is used to illuminate the floaters from the side as shown in Fig. 1(c). The two-dimensional floater positions are recorded with a high-speed camera (Photron Fastcam SA.1) at 500 frames per second. Each image is 546×1030 pixels (38×72 mm²), which covers around 75% of the total cross section area

^{*} cedaysan@gmail.com

[†] d.lohse@utwente.nl

[‡] d.vandermeer@tnw.utwente.nl

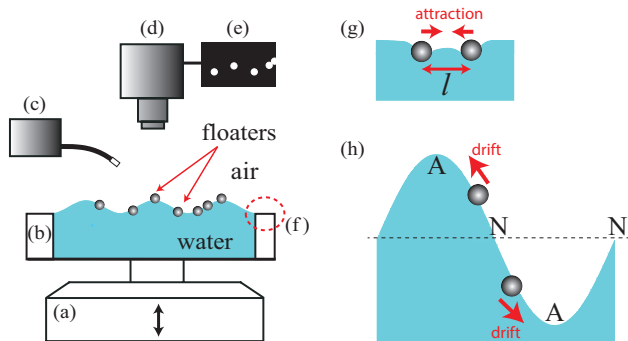


FIG. 1. (color online). Experimental setup: (a) shaker, (b) glass container, $81 \times 45 \times 10 \text{ mm}^3$, (c) Schott fiber light source, (d) Photron Fastcam SA.1 (e) an illustration of a camera image, (f) pinned brim-full boundary condition, (g) the surface deformation around our hydrophilic heavy floaters causes an attractive force, (h) the direction of the period-averaged drift of a single floater, where A and N represent the antinode and the node, respectively.

of the container. The vertical depth of field is taken to be large enough to capture the maximum vertical displacement ($2.5 \pm 0.1 \text{ mm}$) of the floaters.

In the period-averaged context, there are two mechanisms that drive the floaters on the standing Faraday wave. The first one is the attractive capillary interaction [6, 7] due to the surface deformation around the floaters [Fig. 1(g)], which is significant when the distance between the floaters l is smaller than the capillary length $l_c = (\sigma/\rho g)^{1/2}$. Here, σ is the surface tension coefficient of the interface, ρ the liquid density, and g the acceleration of gravity. (For an air-water interface at 20°C , $l_c = 2.7 \text{ mm}$.) The second is due to the standing Faraday wave, which causes a time-averaged drift of the floaters towards the antinodes [Fig. 1(h)], which is observed and described in [1, 3]. This drift, which is discussed in the Supplementary Material [15], bears similarity to a periodic rolling of macroscopic beads on an oscillating plate [16, 17] and is reminiscent of the famous Stokes' drift of an object on a traveling wave.

The control parameter of the experiment is the floater concentration ϕ . We simply measure ϕ by dividing the area covered with floaters by that of the total horizontal field of view. In Fig. 2 we show a top view of the distribution of the particles in two distinct limits, namely for low ϕ and high ϕ . The remarkable difference between the two states is clear: For low ϕ [Fig. 2(a)] small clusters float around the antinodes, whereas for high ϕ [Fig. 2(b)] there is on large cluster around the nodal lines. This completely inverts the pattern and the particles now seen to avoid the antinodal regions.

To inspect this concentration dependent clustering we introduce the correlation factor c , which quantifies to what extent the position of the clusters is correlated with the wave antinodes

$$c \equiv \frac{\langle \phi(\mathbf{r}, t) a(\mathbf{r}) \rangle_{\mathbf{r}, t}}{\langle \phi(\mathbf{r}, t) \rangle_{\mathbf{r}, t}}, \quad (1)$$

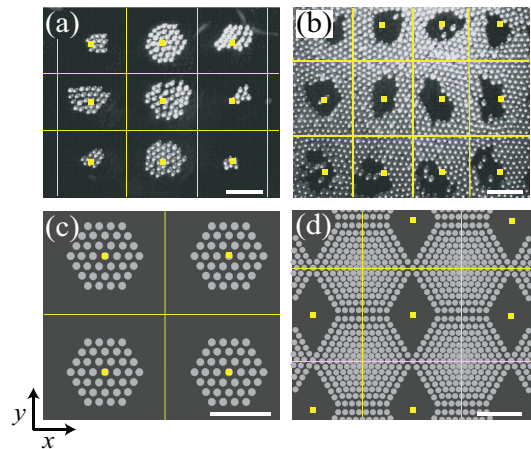


FIG. 2. (color online). (a,b) Clustering of floaters on a rectangular standing wave in experiment. The snapshots show the stationary state when the surface wave elevation is nearly zero. The small yellow rectangles mark the location of the antinodes and the yellow lines that of the nodal lines. Clearly, for $\phi=0.08$ (a) particles cluster at the antinodes, whereas for $\phi=0.61$ (b) the pattern is spontaneously inverted into a large cluster around the nodal lines. Note that in (b) all particles touch whereas the average distance between particles in (a) is somewhat larger. This is due to the breathing effect explained in the text. (c,d) Artificial antinode clusters at $\phi=0.10$ (c) and node clusters at $\phi=0.44$ (d) as used in the potential energy calculation. The white bars indicate a length scale of 5 mm .

where the parentheses $\langle \rangle_{\mathbf{r}, t}$ indicate that the average is taken with respect to both space $\mathbf{r} = (x, y)$ and time t [18]. Here, $\phi(\mathbf{r}, t)$ is the floater concentration and the wave distribution $a(\mathbf{r})$ is a test function which is positive at the antinodes and negative at the nodes. More specifically, $a(\mathbf{r})$ is defined as

$$a(\mathbf{r}) = \begin{cases} \beta a_{\cos}(\mathbf{r}) & \text{when } a_{\cos}(\mathbf{r}) > 0 \text{ (antinodes),} \\ a_{\cos}(\mathbf{r}) & \text{when } a_{\cos}(\mathbf{r}) < 0 \text{ (nodes).} \end{cases} \quad (2)$$

Here, $a_{\cos}(\mathbf{r}) = 2 \cos^2 k_x x \cos^2 k_y y - 1$, with k_x, k_y the wave numbers in the x, y -direction. Since with the above definition the nodal regions are three times as small as the nodal ones, a constant $\beta = 3$ is introduced such that $c = 0$ when the floaters are equally distributed over the two-dimensional wave surface [19]. To check the robustness of c regarding the precise form of $a(\mathbf{r})$, we also use a step function $a_{\text{step}}(\mathbf{r})$, which equals 1 at the antinodes and -1 at the nodes.

In Fig. 3(a) we present the correlation factor c plotted against ϕ for both a_{\cos} and a_{step} . We observe three distinct regions: For low ϕ (< 0.2) the clear positive value of c indicates the presence of the antinode clusters (region I). Secondly for very high ϕ (> 0.5) we find node clusters for which $c < 0$ (region III). Finally, there is a broad intermediate region II, in which we observe morphologically rich self-organized floater patterns, some of which steadier than others. These quasi-steady patterns cause the large scatter in c in the region between $\phi = 0.2$ and 0.35 . Between $\phi = 0.35$ and 0.5 , patterns are quite

dynamic leading to an even spreading of particles over the waves ($c \approx 0$).

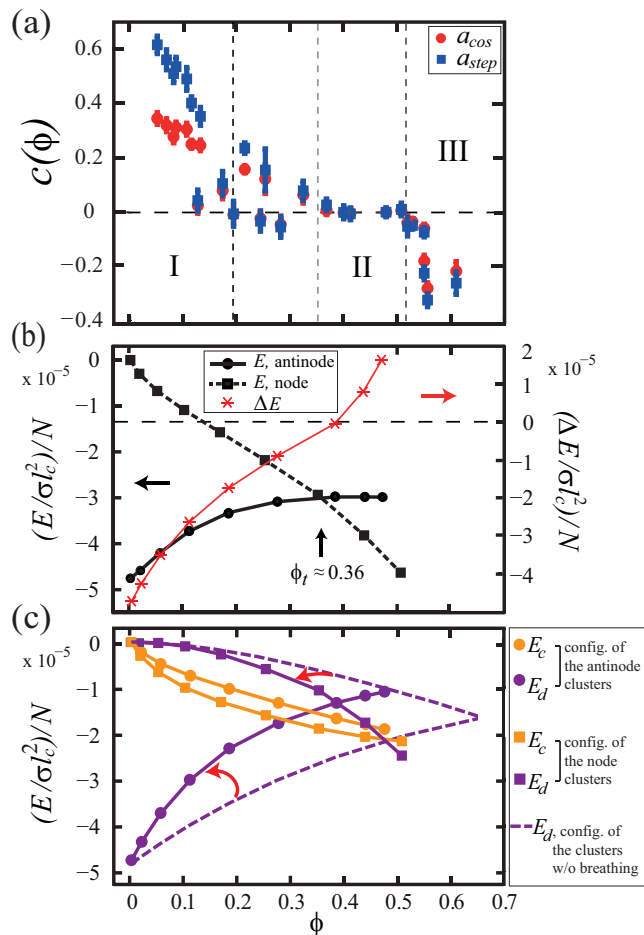


FIG. 3. (color online). Experimental (a) and calculated (b, c) transition from antinode to node clusters. (a) The correlation factor c is plotted versus the floater concentration ϕ for both a_{cos} [red circles] and a_{step} [blue squares], where the error bars indicate the standard deviation of a single experiment. (b) The total potential energy E/N per floater particle for the artificial patterns [see Fig. 2(c,d)], non-dimensionalized by σl_c^2 , is plotted versus ϕ for both the antinode [black circles] and node [black squares] configurations. $\Delta E/N$ [red stars] represents the energy difference between the antinode and node configurations. (c) Constituents of E/N versus ϕ . Circles indicate the capillary energy E_c/N [orange] and the drift energy E_d/N [purple] for the antinode configurations, whereas squares indicate the same quantities for the node clusters. For comparison, the purple dashed lines show the drift energy E_d without incorporating the breathing effect.

In addition to the position, another remarkable difference between the antinode and the node clusters is hidden in their dynamics during a single wave period: Experimentally we observe that in the antinode clusters the floaters periodically move away from and towards the antinode [Fig. 4(a)]. This happens because when the wave reaches its maximum the (downward moving) floaters move away from the antinode, whereas in the minimum they move towards it. We call this periodic

motion at the antinode clusters *breathing* [15]. In contrast, nodal clusters do not breathe; instead the clusters as a whole oscillate back and forth around the nodal lines [Fig. 4(b)]. As a result, the floaters in the node clusters stay closely together without changing their relative distance (which is approximately equal to the particle diameter $2R$), whereas the period-averaged distance between the particles in the antinode cluster is significantly larger than $2R$ [20].

Potential energy estimate – Now, what is the reason for the observed pattern inversion? To answer this question we estimate the energy in artificially created node and antinode clusters that are inspired by our experimental observations [Fig. 4(a, b)]: The antinode cluster is modeled as a two-dimensional static hexagonally packed cluster where the distance between the neighboring floaters increases towards the antinode point (A) [Fig. 4(c)] to implement the observed breathing effect. The distance here can be considered as the period-averaged experimental distance between the floaters. The node cluster, in contrast, is designed as a two-dimensional hexagonal cluster where the distance between the neighboring floaters sitting exactly at the crossing of two nodal lines (N) is equal to an average floater diameter $2R$ [Fig. 4(d)]. Furthermore, the distance slightly increases away from N [21].

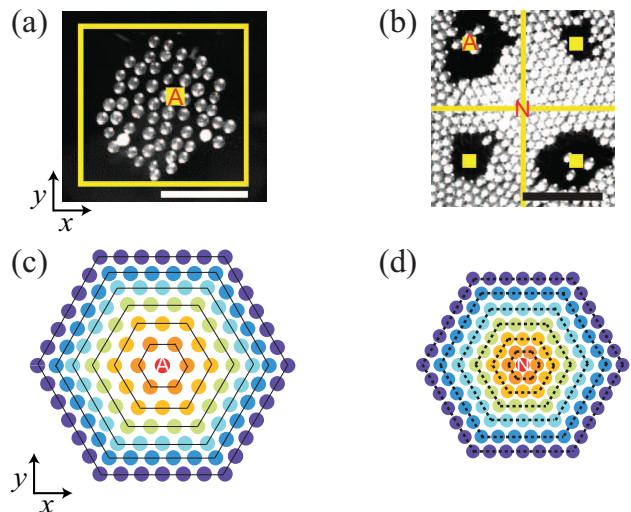


FIG. 4. (color online). The breathing effect: When we compare an experimental antinode (a) with a node cluster (b), we clearly see that particles in the first are much farther apart due to breathing (see text). Again, the antinodes (A) are marked by small yellow rectangles and the nodes (N) with yellow lines. The bars indicate a length scale of 5 mm. We artificially design hexagonal clusters to incorporate this breathing effect: an antinode cluster (c) is grown by adding hexagonal rings at decreasing increments r_{nn} starting from a large initial value, whereas a node cluster (d) is grown from a close-packed hexagonal structure with increasing increments r_{nn} [21]. The color coding identifies consecutive rings.

During the motion of the floaters on the wave there is

an intricate exchange of wave energy (input), potential energy, kinetic energy and dissipation (output). However, in a steady state the in- and output must balance and since the particles return to (approximately) the same positions after each period of the wave it is sufficient to compare the potential energy E of the floaters for the two situations. This potential energy has two contributions, due to the drift and due to the capillary attraction.

The first contribution to E is the capillary energy E_c , which we estimate as the sum of the capillary energies of each floater pair $E_c(l_{i,j})$, where $l_{i,j}$ is the distance between floaters i and j . Here, we use the approximation $E_c(l_{i,j}) = A_c K_0(l_{i,j}/l_c)$, where K_0 is the zeroth order modified Bessel function of the second kind. This approximation is valid for small surface deformations, i.e., for small spheres, loosely packed structures or relatively distant spheres [6, 7]. Studies that comparatively discuss the exact solution of the capillary force of floaters of similar size suggest that the difference with the approximation is less than 2% [23, 24]. The second contribution to E is the drift energy E_d . It is the sum over the single-floater drift energy $E_d(x_i, y_i) = A_d(1 - \cos 2k_x x_i)(1 - \cos 2k_y y_i)$, where (x_i, y_i) is the position of floater i . Note that the prefactors A_c and A_d are known functions of particle, liquid and wave properties and are provided in the supplementary material [25].

Subsequently, we use the above expressions to estimate the potential energy E in our antinode and node cluster configurations (Fig. 2(c, d)) as a function of the floater concentration ϕ (i.e., the number of particles N) and compare them in Fig. 3(b). For increasing ϕ , the energy per floater E/N increases for the antinode clusters, whereas it decreases for the node clusters. As a result, there is a crossover $\phi_t \approx 0.36$ separating a low ϕ region, where the antinode clusters are energetically favorable, from a high ϕ one, where the node clusters have lower potential energy. In addition, ϕ_t lies in the transition region of Fig. 3(a) and is therefore in agreement with the experiment.

To examine the physical reason for this crossover, in Fig. 3(c) we turn to the constituents of E , namely E_c and E_d . For the capillary energy E_c there is hardly any difference between the node and antinode clusters, except for a slightly milder decrease for the latter, caused by the larger average distance between the floaters due to the breathing.

Things are very different for the drift term: For small ϕ the node clusters initially have a high drift energy E_d/N per floater and the antinode clusters are favorable. When we increase ϕ without including the

breathing effect –i.e., both clusters are just hexagonally packed with nearest neighbor distance $2R$ – the energy per floater in the node clusters decreases and that of the antinode clusters increases until they meet for a very high value of ϕ , corresponding to an almost completely floater-covered surface [dashed lines in Fig. 3(c)]. However, when we do include the breathing effect in our calculation, E_d/N increases much faster for the antinode cluster due to the large average distance of the particles near the antinodes. Similarly, E_d/N increases somewhat more rapidly for the nodal clusters. The result is that the crossover shifts to a moderate value of ϕ , namely $\phi_t \approx 0.36$. This implies that nodal clusters now already become energetically favorable when the surface is not yet covered with particles, which causes the inverted patterns to exist.

Conclusion – In summary, in this Letter we study the role of the floater concentration ϕ on the spatial distribution of macroscopic spheres floating on a standing Faraday wave. For low ϕ , we experimentally observe that hydrophilic heavy floaters form clusters at the antinodes, suggested by the theory [1, 3]. For high ϕ , the same floaters unexpectedly self-organize into the *inverse* pattern, namely a large cluster around the nodal lines of the wave. To understand such a collective behavior, we calculate the potential energy of the floater system and are able to explain our observations in both limits. More specifically, the transition point ϕ_t obtained from our energy calculation lies within the experimental transition region.

We find that the observed breathing effect is essential for the existence of the crossover. The breathing creates a significant difference in the drift energy such that the node clusters are energetically favorable already when only drift energy is taken into account. The role of the capillary interaction is just to keep the floater particles self-organized in rafts; without this attractive interaction the floaters would be freely drifting around instead of forming clusters.

Whereas our potential energy argument nicely accounts for the existence of the stable antinode and node patterns, it is not able to capture the large transitional region that was observed between $\phi = 0.2$ and 0.5 . Presumably, what happens in this region is that the antinode clusters become too large to stay pinned at the antinode regions and start to wander into the nodal regions under the influence of the wave motion. Characterizing these patterns will be the objective of a future paper.

The work is part of the research program of FOM, which is financially supported by NWO.

[1] G. Falkovich, A. Weinberg, P. Denissenko, and S. Lukashuk, *Nature (London)* **435**, 1045 (2005).
 [2] P. Denissenko, G. Falkovich, and S. Lukashuk, *Phys. Rev. Lett.* **97**, 244501 (2006).

[3] S. Lukashuk, P. Denissenko, and G. Falkovich, *Eur. Phys. J. Special Topics* **145**, 125 (2007).
 [4] In this case, both heavy hydrophilic and hydrophobic spheres can float by the help of surface tension.

- [5] P. Cicuta and D. Vella, *Phys. Rev. Lett.* **102**, 138302 (2009).
- [6] D. Vella and L. Mahadevan, *Am. J. Phys.* **73**, 817 (2005).
- [7] D. Y. C. Chan, J. D. Henry, Jr., and L. R. White, *J. Colloid Interface Sci.* **79**, 410 (1981).
- [8] M. Berhanu and A. Kudrolli, *Phys. Rev. Lett.* **105**, 098002 (2010).
- [9] C. Planchette, E. Lorenceau, and A.-L. Biance, *Soft Matter* **8**, 2444 (2012).
- [10] S. Douady, *J. Fluid Mech.* **221**, 383 (1990).
- [11] The particles have been custom made and are not commercially available.
- [12] See Section 1.1 of the Supplementary Material for further information on the calculation of the contact angle of the floater.
- [13] C. Duez, C. Ybert, C. Clanet, L. Bocquet, *Nat. Phys.* **3**, 180 (2007).
- [14] See Section 4 of the Supplementary Material for details of the procedure for creating a standing Faraday wave in the presence of floaters.
- [15] See Section 1.2 of the Supplementary Material for the discussion on the direction of the single-floater time-averaged drift for our hydrophilic heavy spheres. In addition, the time-dependent drift mechanism is introduced.
- [16] H. J. van Gerner, M. A. van der Hoef, D. van der Meer, and K. van der Weele, *Phys. Rev. E* **82**, 012301 (2010).
- [17] H. J. van Gerner, K. van der Weele, M. A. van der Hoef, and D. van der Meer, *J. Fluid Mech.* **689**, 203 (2011).
- [18] The spatial average is performed over the total horizontal field of view and the time average is computed using the experimental images over 200 wave periods ($\approx 200 \times 0.05 = 10$ s).
- [19] In this procedure the patterns are shifted such that the origin coincides with an antinode. To eliminate the contribution of floater motion into the third dimension, only images where the wave elevation is nearly zero are used in the average.
- [20] See the Supplementary Movie for a video presenting the breathing antinode clusters at low ϕ and the non-breathing node clusters at high ϕ floating on the standing Faraday wave.
- [21] See Section 2 of the Supplementary Material for further details on the artificial antinode and node cluster configurations.
- [22] Both the size and the density of a sphere are important in judging whether the linear approximation is applicable. To this end, we check the Bond number B for our spheres and find that $B \ll 1$, *i.e.*, the approximation is valid. (See Section 1.1 of the Supplementary Material.)
- [23] N. D. Vassileva, “Behavior of 2D aggregates in shear flow”, PhD Thesis, Physics of Complex Fluids Group, University of Twente (2006).
- [24] N. D. Vassileva, D. van den Ende, F. Mugele, and J. Mellema, *Langmuir* **21**, 11190 (2005).
- [25] The full expressions for $E_c(l_{i,j})$ and $E_d(x_i, y_i)$, including prefactors, are provided in the Supplementary Material Section 3.